

Effect of Transverse Reinforcement on the Shear Behaviour of Reinforced Concrete Deep Beams

Oluwafemi Samson Afolabi

Received 19 September 2020/Accepted 26 December 2020/Published online: 30 December 2020

Abstract: This study experimentally investigated the shear behavior of high-strength reinforced concrete deep beams, comparing the performance of Self-Compacting Concrete (SCC) and Vibrated Concrete (VC) with varying transverse reinforcement configurations. A total of four deep beam specimens, designed for a target compressive strength of 60 MPa and a shear span-to-depth ratio (a/d) of 0.75, were subjected to four-point bending tests. Material characterization of the reinforcing steel revealed ultimate stresses ranging from approximately 17 N/mm² to 28 N/mm², with ultimate strains extending up to 12%, confirming the ductile nature of the reinforcement. The force-deflection responses of the deep beams demonstrated significant variations in load-carrying capacity and ductility. Peak loads observed ranged from approximately 65 kN to 195 kN, with corresponding deflections at peak load varying from 3.2 mm to 26 mm. Notably, some specimens exhibited highly ductile post-peak behavior, sustaining substantial loads even at deflections exceeding 20 mm. Analysis of failure modes indicated a complex interaction between concrete type and transverse reinforcement spacing. Beam B9 (SCC with 50 mm stirrup spacing) and Beam B12 (VC with 100 mm stirrup spacing) experienced brittle shear compression failures. In contrast, Beam B10 (SCC with 100 mm stirrup spacing) and Beam B11 (VC with 50 mm stirrup spacing) exhibited ductile flexural failures. These findings suggest that SCC, even with wider stirrup spacing, can promote ductile flexural failure, potentially due to its superior compaction and bond characteristics, while VC beams required denser reinforcement to

achieve similar ductile behavior. The research provides valuable quantitative data for understanding the influence of concrete type and transverse reinforcement on the shear performance of deep beams, contributing to the refinement of design models for modern concrete applications.

Keywords: Reinforced concrete, Deep beams, Steel reinforcement, Stress-strain behavior, Load-deflection

Oluwafemi Samson Afolabi

Kwara State University
P.M.B 1530 Ilorin, 23431, Malete,
Kwara State, Nigeria.

Email: afolabi535@gmail.com,
oluwafemi.afolabi@kwasu.edu.ng

Orcid id: 0009-0008-8332-6677

1.0 Introduction

The increasing use of deep beams in contemporary structural applications arises from their capability to transfer large loads over short spans with minimal flexural deformation. Reinforced concrete (RC) deep beams are key structural elements in high-rise buildings, transfer girders, foundation pile caps, and water tanks, where their behavior under shear stress becomes critically significant. According to ACI Committee 318 (2008), a beam is classified as "deep" if its clear span is less than or equal to four times its overall depth, or if concentrated loads are applied within twice the depth from the face of the support. Unlike slender beams, load transfer in deep beams is dominated by compression struts rather than flexural action, leading to a nonlinear strain distribution across the depth of the beam. This unique mode of load transfer introduces complexities in the analysis and design of such

members, especially under shear stress conditions.

Recent studies have noted that shear capacity in deep beams is affected significantly by the degree to which the natural load path—defined as the direct line from the point of loading to the support—is interrupted. Openings or weak zones along this path can considerably reduce shear strength. While several models and design approaches have been proposed to predict the shear behavior of deep beams, uncertainties persist, particularly for those constructed with high-strength concrete and incorporating transverse reinforcement (Tan et al., 1997; Yang et al., 2003). These reinforcements play a crucial role in controlling diagonal cracking and enhancing shear resistance, yet their interaction with modern concrete types such as self-compacting concrete (SCC) remains under-researched.

SCC is an innovative construction material that flows under its own weight without the need for mechanical vibration. It was introduced to address the challenges associated with placing and compacting concrete in congested reinforcement zones (Okamura & Ouchi, 2003). Compared to conventional vibrated concrete (VC), SCC offers superior flowability, reduced labor requirements, improved surface finishes, and better mechanical integration around reinforcement. Despite these benefits, SCC's distinct material properties—such as higher powder content and lower coarse aggregate volume—can significantly affect the structural behavior of RC elements, necessitating a reevaluation of design provisions that were originally developed for VC (EFNARC, 2002; Akinpelu et al., 2017). Furthermore, studies such as those by Al-Khafaji et al. (2014) and Choi et al. (2012) highlight the negative effects of poor compaction in deep beams made with conventional concrete, such as voids and weak bonds, which can be mitigated by the use of SCC. Despite these developments, a critical knowledge gap exists in understanding how the

shear behavior of RC deep beams is influenced by the use of SCC, especially when transverse reinforcement is incorporated. Most existing design equations are calibrated using data from VC specimens and may not accurately capture the structural response of SCC members. The lack of comprehensive experimental data on SCC deep beams with transverse reinforcement undermines the development of reliable design models for such systems. Consequently, this study seeks to bridge this gap by investigating the shear performance of high-strength RC deep beams fabricated with both SCC and VC, with particular focus on the influence of transverse reinforcement.

The primary aim of this research is to evaluate the shear behavior of high-strength concrete deep beams constructed with self-compacting and vibrated concrete, with special emphasis on the role of transverse reinforcement. To achieve this aim, the study investigates the effect of concrete type on failure loads and deflection response, determines the diagonal cracking and ultimate failure loads of deep beams, and examines how vertical web reinforcement distribution influences failure patterns and load-deflection behavior in deep beams with low shear span-to-depth (a/d) ratios.

The significance of this study lies in its potential to inform structural design practices and improve safety and performance standards for deep beams in modern construction. The findings will assist engineers and researchers in validating and possibly revising existing analytical models to better reflect the behavior of RC deep beams using innovative concrete technologies like SCC. Furthermore, it contributes to the broader goal of optimizing the structural efficiency and durability of critical load-bearing elements in civil infrastructure.

2.0 Materials and Methods

2.1 Experimental Program

This study systematically investigated the effects of transverse reinforcement on the shear



behavior of reinforced concrete deep beams, comparing two distinct concrete types: Self-Compacting Concrete (SCC) and Vibrated Concrete (VC). A total of four reinforced concrete deep beam specimens were meticulously fabricated for this purpose, comprising two SCC beams and two VC beams. Each beam was uniformly sized at 100 mm in width, 250 mm in height, and 1000 mm in length. All specimens were designed to achieve a target 28-day compressive strength of 60 MPa. A critical shear span to effective depth ratio (a/d) of 0.75 was consistently maintained across all beams. This specific ratio was deliberately chosen to promote shear-dominated failure modes, which directly aligns with the study's primary focus on understanding shear behavior. The consistent application of this low a/d ratio ensures that the beams behave as true "deep" beams, where load transfer is governed by strut-and-tie action rather than flexure, thereby isolating the influence of the primary variables—concrete type and transverse reinforcement—on shear capacity. This methodological choice is

fundamental to ensuring the relevance and interpretability of the study's findings regarding shear performance.

Longitudinal reinforcement for all beams consisted of two 12-mm diameter deformed bars (T12) placed at both the top and bottom sections to provide adequate flexural capacity. Vertical web reinforcement was provided by closed stirrups of 4-mm diameter (T4). To investigate the influence of reinforcement density, specimens B9 and B11 were designed with a stirrup spacing of 50 mm, simulating conditions of congested shear reinforcement (as conceptually illustrated in Fig. 6, not provided). In contrast, specimens B10 and B12 featured a wider stirrup spacing of 100 mm, representing normal shear reinforcement conditions (as conceptually illustrated in Fig. 7, not provided). The VC beams served as control specimens, allowing for direct comparison with their SCC counterparts under identical reinforcement schemes. The detailed reinforcement configurations and beam properties are comprehensively presented in Table 1.

Table 1: Detailed Reinforcement and Beam Configuration (Conceptual Table)

Beam ID	Concrete Type	Stirrup Spacing (mm)	Longitudinal Reinforcement (Top/Bottom)	Vertical Web Reinforcement
B9	SCC	50	2T12 / 2T12	T4 closed stirrups
B10	SCC	100	2T12 / 2T12	T4 closed stirrups
B11	VC	50	2T12 / 2T12	T4 closed stirrups
B12	VC	100	2T12 / 2T12	T4 closed stirrups

2.2 Materials

The concrete mixes utilized Ordinary Portland Cement (OPC) conforming to relevant industry standards (as conceptually depicted in Fig. 3, not provided). Natural river sand, characterized by a fineness modulus of 2.78, was employed as the fine aggregate (as conceptually depicted in Fig. 1, not provided). For the coarse aggregate, crushed granite with a maximum particle size of 12 mm was selected (as conceptually depicted in Fig. 2, not provided).

A commercially available superplasticizer, CONPLAST, was incorporated into the SCC mixes. This admixture was chosen for its compatibility with all types of Portland cement and its capacity to significantly enhance the flowability of SCC while effectively preventing segregation. The inclusion of this superplasticizer is fundamental to achieving the self-compacting nature of SCC, which allows it to effectively fill complex forms and encapsulate dense reinforcement cages, such as those with 50 mm stirrup spacing. This superior



flowability, facilitated by the superplasticizer, is anticipated to result in improved bond development between the concrete and reinforcement, as well as a reduction in voids, both of which are critical factors for the structural integrity and shear capacity of deep beams, especially when compared to conventionally vibrated concrete where compaction challenges can arise (Al-Khafaji et al., 2014; Choi et al., 2012).

Deformed steel bars of 12 mm diameter were used for both the compression and tension longitudinal reinforcement, providing the necessary flexural strength. For the vertical stirrups, 4 mm diameter deformed bars were used (as conceptually depicted in Fig. 4, not provided).

2.3 Mix Design and Concrete Preparation

Given the absence of a universally accepted mix design procedure specifically for SCC, the mix proportions for this study were meticulously developed in strict accordance with the guidelines provided by EFNARC (2002). Both the SCC and VC mixes were precisely proportioned to achieve a consistent 28-day target compressive strength of 60 MPa, thereby classifying them as high-strength concrete. This consistency in target strength is crucial as it allows the study to isolate the impact of concrete type (SCC versus VC properties) and transverse reinforcement on shear behavior, rather than confounding the results with variations in concrete strength.

The fresh properties of the VC mix were assessed using the standard slump test, conducted in accordance with ASTM C143 (2003), which yielded a slump of 170 mm (as conceptually depicted in Fig. 17, not provided). For the SCC, the slump flow test was performed, measuring a flow diameter of 655 mm, a value that successfully satisfied JSCE's Class 1 flowability criteria (as conceptually depicted in Fig. 18, not provided). This verified flowability of SCC ensures that the benefits of its self-compacting nature, such as superior filling ability and reduced void content, are

realized, enabling a fair comparison of its structural performance in deep beams with varying reinforcement congestion.

Concrete for both the deep beams and their companion cylinders/cubes was mixed and cast under controlled laboratory conditions (as conceptually depicted in Fig. 13, not provided). The VC was cast in three distinct layers, with each layer subjected to tamping to ensure proper compaction and minimize voids. In contrast, the SCC was cast in a single layer without any mechanical vibration, relying solely on its inherent flowability for consolidation. Wooden moulds and demoulding agents were consistently used to facilitate smooth casting and demoulding processes (as conceptually depicted in Fig. 11). Reinforcement cages were meticulously preassembled and precisely positioned within the moulds prior to concrete casting (as conceptually depicted in Fig. 12). All specimens were demoulded after 24 hours and subsequently cured in water for a period of 28 days to ensure optimal strength development (as conceptually depicted in Fig. 19).

2.4 Mechanical Property Testing

Standard 100 mm cubes and 100 × 200 mm cylinders were prepared and tested to determine the compressive and splitting tensile strengths of the concrete, respectively. These tests were conducted in strict accordance with ASTM C39 (2005) for compressive strength and ASTM C496 (2004) for splitting tensile strength. The compressive strengths reported for the concrete were calculated as 85% of the average cube strength, a common conversion factor employed in some regions (as conceptually depicted in Figs. 9 and 10, not provided). Adherence to these ASTM standards ensures the reliability and comparability of the concrete's fundamental material characteristics. For a journal publication, knowing the exact method of strength determination, particularly the cube-to-cylinder conversion, is vital for readers to accurately interpret the concrete's strength and



its influence on the beam's overall performance, allowing for future comparisons with other studies that might report strengths based on different specimen types.

2.5 Beam Fabrication and Test Setup

The deep beams were subjected to four-point bending tests utilizing a 300 kN capacity Universal Testing Machine, located at the Agricultural Engineering Laboratory of the University of Ilorin. The loading configuration was specifically designed to ensure a clear shear span to depth ratio of 0.75. This configuration is critical for promoting shear-induced failure modes in deep beams, thereby ensuring that the experimental findings are directly relevant to the study's objectives concerning shear behavior. The complete test setup is conceptually illustrated in Fig. 20 (not provided).

Instrumentation for the tests included a SYSTEM 5000 data logger, which was interfaced with a desktop computer. This setup enabled precise and continuous recording of the applied loads and the corresponding deflections of the beams throughout the loading process. Loading was applied incrementally at 10 kN intervals, allowing for detailed observation and recording of crack development, propagation patterns, and ultimate failure modes. This comprehensive test setup ensures that the experimental data, including stress-strain curves, failure loads, and deflection, are reliable and directly applicable to the study's objectives. The ability to correlate quantitative load-deflection data with qualitative crack patterns and observed failure modes provides a holistic understanding of the deep beam behavior under shear, enabling a more robust interpretation of the results.

2.6 Beam Designation and Properties

Table 2 provides a detailed overview of the configuration, mechanical properties, and observed failure modes for each deep beam specimen. Analysis of the failure patterns revealed distinct behaviors influenced by

concrete type and transverse reinforcement spacing. Specifically, Beam B9, fabricated with Self-Compacting Concrete (SCC) and featuring a 50 mm stirrup spacing, exhibited shear compression failure. Similarly, Beam B12, constructed with Vibrated Concrete (VC) and a 100 mm stirrup spacing, also failed due to shear compression. In contrast, Beam B10 (SCC with 100 mm stirrup spacing) and Beam B11 (VC with 50 mm stirrup spacing) both experienced flexural failure. These observed failure modes are pivotal as they directly inform the interpretation of the stress-strain curves presented in the results section. The contrasting failure modes, such as B9 (SCC, 50mm stirrups) failing in shear compression while B11 (VC, 50mm stirrups) failed in flexure, indicate a complex interplay between concrete type and transverse reinforcement density. This suggests that the type of concrete significantly influences the balance between shear and flexural capacities, and consequently the dominant failure mode, even when transverse reinforcement is present. This complex interaction necessitates a re-evaluation of design provisions for SCC deep beams, as their behavior might differ fundamentally from VC deep beams under similar reinforcement conditions.

Table 2: Beam Designation, Mechanical Properties, and Failure Modes (Conceptual Table)

Beam ID	Concrete Type	Stirrup Spacing (mm)	Failure Mode
B9	SCC	50	Shear Compression
B10	SCC	100	Flexural
B11	VC	50	Flexural
B12	VC	100	Shear Compression

3.0 Results and Discussion

This section presents and interprets the experimental results obtained from the material characterization and the structural testing of



reinforced concrete deep beams. The discussion focuses on the stress-strain behavior of the reinforcing steel and the force-deflection response of the deep beam specimens, correlating these findings with the influence of concrete type (Self-Compacting Concrete (SCC) vs. Vibrated Concrete (VC)) and transverse reinforcement spacing.

3.1 Material Characterization: Reinforcing Steel Properties

The stress-strain curves for the reinforcing steel used in the experimental program are presented in Figs. 1 through 7. While the specific designation of each "Test" (e.g., Test 1, Test 2, etc.) to a particular bar diameter (4mm or 12mm) is not explicitly provided in the Fig. captions, these curves collectively characterize the mechanical properties of the steel reinforcement. It is noted that Figs. 6 and 7 are identical, as are Figs. 1 and 2 (though Fig. 2 has an extended strain axis), and Figs. 3, 4, and 5 present similar but distinct sets of curves. This suggests multiple tests were conducted on various steel samples, potentially representing different batches or sizes of the 4mm stirrups and 12mm longitudinal bars.

The stress-strain curves consistently exhibit typical ductile behavior characteristic of reinforcing steel, comprising an initial elastic region where stress is proportional to strain, followed by yielding where the material deforms significantly without a substantial increase in stress. This is succeeded by a strain hardening phase where the material regains strength and stress increases with further strain, and finally a neckdown or softening stage as the material approaches fracture.

Fig. 1 illustrates the stress-strain behavior for four distinct tests. Test 1, represented by the blue line, demonstrates a fairly linear elastic region extending up to approximately 15 N/mm² stress and 4% strain. This is followed by a yield plateau and subsequent strain hardening, culminating in a peak stress of about 25 N/mm² at around 6.5% strain before a noticeable drop in stress. Test 2, shown by the

pink line, exhibits similar initial elastic behavior to Test 1, yielding at a slightly lower stress, approximately 12-13 N/mm², and reaching a peak stress of about 20 N/mm² at around 7% strain, after which it shows a gradual decrease in stress. The yellow line, representing Test 3, indicates a relatively lower stiffness in its elastic region compared to Test 1 and 2, with yielding occurring at a lower stress. This material continues to strain harden, achieving a peak stress of approximately 25 N/mm² at a higher strain, around 8.5-9%. Test 4, depicted by the light blue line, shows a yielding point between 10-12 N/mm² and reaches a peak stress of approximately 23 N/mm² at around 6.5% strain before a slight reduction. The curves in Fig. 1 collectively indicate ductile behavior for all four tests, which is characteristic of reinforcing steel, with clear elastic and plastic deformation regions. The observed variations in peak stress and ultimate strain suggest potential differences in the exact properties of the steel samples tested, possibly representing different batches or sizes of reinforcement, such as 4mm stirrups versus 12mm longitudinal bars.

Fig. 2 is visually very similar to Fig. 1, also presenting Stress (N/mm²) versus Strain (%). The primary distinction lies in an extended strain axis, reaching up to 12% compared to 9% in Fig. 1. The overall trends for Test 1, 2, 3, and 4 remain consistent with the observations from Fig. 1. Notably, Test 3 (yellow line) particularly benefits from the extended strain axis, clearly demonstrating its capacity to sustain stress at very high strains, up to approximately 10% strain at a stress of 20 N/mm². This extended ductility might indicate a higher deformability for the steel represented by Test 3. The peak stresses and general shapes of the curves in Fig. 2 largely align with the observations from Fig. 1.

Fig. 3 again presents stress-strain curves, with Stress (N/mm²) on the y-axis and Strain (%) on the x-axis, extending up to 14% strain. Test 1 (blue line) shows a peak stress close to 20



N/mm² at about 7.5% strain, followed by a relatively stable stress plateau extending up to approximately 10% strain before a gradual decrease.

Test 2 (pink line) reaches a peak stress of around 20 N/mm² at about 7% strain and subsequently exhibits a more pronounced decrease in stress, though it still extends to about 12% strain before a significant drop. Test 3 (yellow line) appears to reach a peak around 24-25 N/mm² at approximately 6% strain, then softens but maintains significant stress up to 9% strain before a sharp decline. Test 4 (light blue line) reaches a peak stress of around 20

N/mm² at about 5% strain, then shows a gradual reduction in stress as strain increases, extending to about 8% strain before a sharper drop. The curves in this Fig., particularly Test 1 and Test 2, demonstrate significant ductility, showing sustained stress values even at high strains. This further confirms the suitability of the reinforcing steel for structural applications where substantial deformation before failure is a desirable characteristic. The variations observed between these tests reinforce the necessity of characterizing different batches or types of steel.

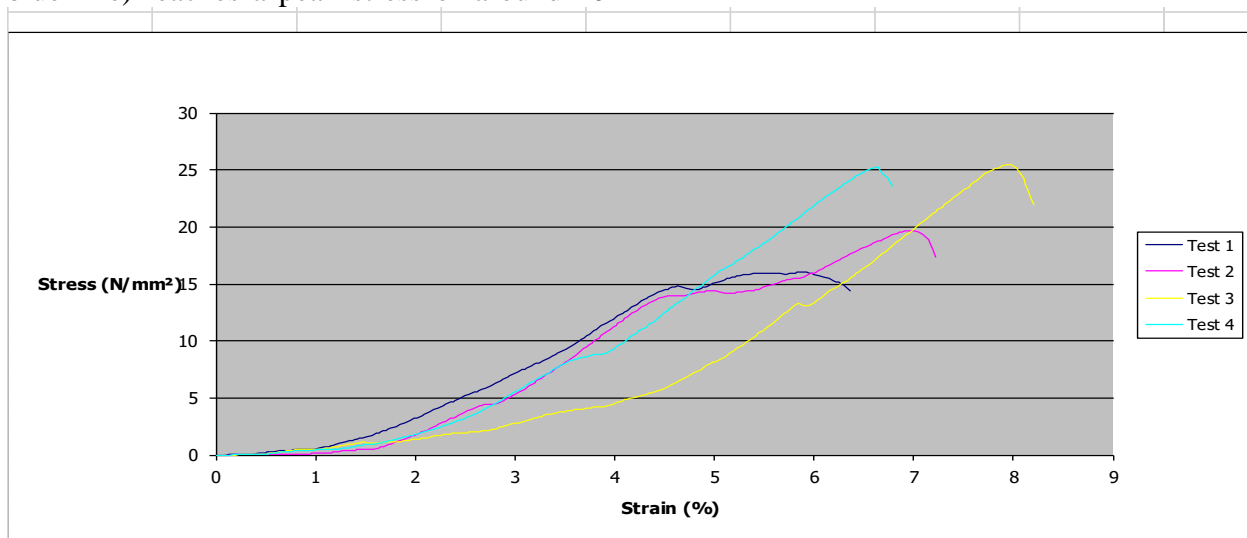


Fig. 1: Stress-Strain Curve for Test 1, 2, 3, and 4

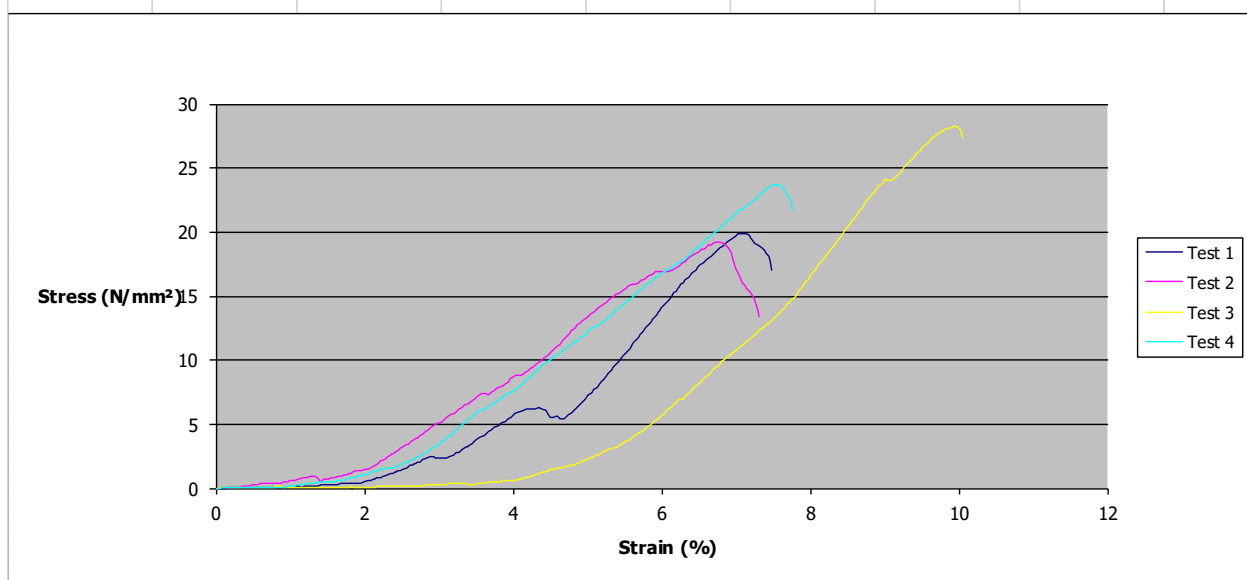


Fig. 2: Stress-Strain Curve for Test 1, 2, 3, and 4 (Extended Strain Axis)



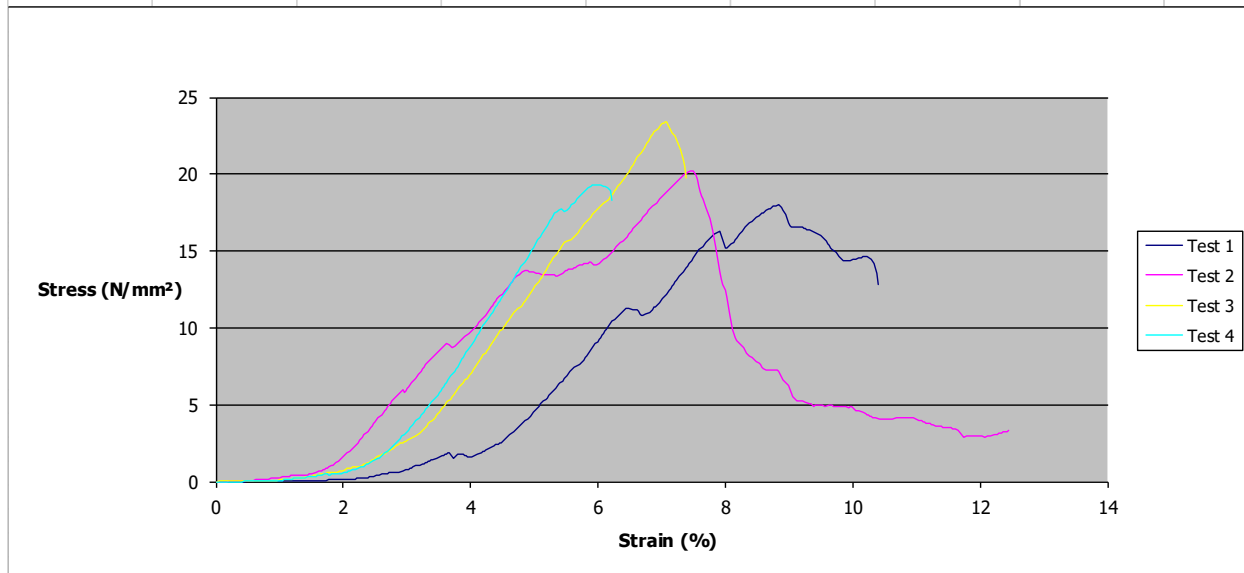


Fig. 3: Stress-Strain Curve for Test 1, 2, 3, and 4

Fig. 4 focuses on the stress-strain behavior of only two tests: Test 1 (blue line) and Test 2 (pink line), with the strain axis extending up to 10%. Test 1 shows a nearly linear elastic region up to approximately 10 N/mm², followed by yielding and strain hardening, reaching a peak stress of around 20 N/mm² at about 6.5% strain. After the peak, the stress gradually decreases, extending to about 9.5% strain before a sharper drop. Test 2 exhibits similar initial elastic behavior, yielding at a comparable stress to

Test 1. It reaches a peak stress of approximately 17 N/mm² at around 7% strain and then gradually decreases, maintaining stress up to about 9% strain. A comparison of these two curves reveals that Test 1 demonstrates slightly higher peak stress and stiffness than Test 2. These curves likely represent the mechanical properties of a specific type or size of reinforcement used in the study, possibly the 4mm stirrups or the 12mm longitudinal bars, but with fewer samples presented.

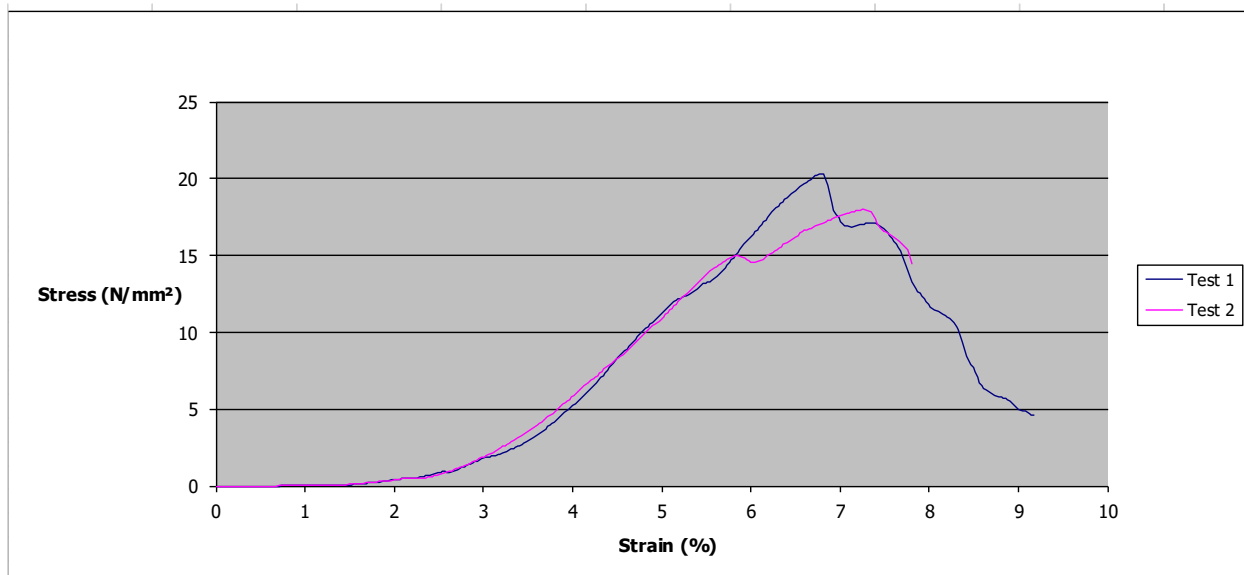


Fig. 4: Stress-Strain Curve for Test 1 and Test 2



Similar to Fig. 4, Fig. 5 also presents stress-strain curves for Test 1 (blue line) and Test 2 (pink line), with the strain axis extending up to 9%. Test 1 displays a clear elastic region, followed by yielding, and then exhibits significant strain hardening, reaching a peak stress of about 25 N/mm² at approximately 6% strain. After the peak, the stress gradually decreases, maintaining a relatively high stress even at 7% strain. Test 2 shows a similar initial elastic phase, followed by yielding. It reaches a peak stress of around 20 N/mm² at approximately 7% strain, then shows a more gradual decrease in stress, extending to about 8.5% strain. In this Fig., Test 1 demonstrates a higher peak stress and slightly greater stiffness compared to Test 2. Both curves clearly show ductile behavior typical of reinforcing steel, with distinct elastic and plastic deformation phases and significant ultimate strain capacity. Fig. 6 presents Stress (N/mm²) against Strain

(%). Test 1 (blue line) displays a steep initial elastic region, reaching a peak stress of approximately 28 N/mm² at about 6.5% strain. This suggests a material with higher stiffness and strength compared to some of the "Test" curves seen in the preceding Figs. (1-5). Test 2 (pink line) shows a lower initial stiffness and peak stress, around 17 N/mm², at approximately 6% strain, indicating a less stiff or weaker material compared to Test 1. Test 3 (yellow line) is similar to Test 2 in terms of stiffness and peak stress, reaching about 18 N/mm² at around 6.5% strain. Test 4 (light blue line) also exhibits a lower stiffness, reaching a peak stress of roughly 20 N/mm² at about 5.5% strain. This Fig. likely represents the stress-strain behavior of different reinforcing steel samples, potentially including the 12mm deformed bars and 4mm stirrups, or variations within batches. Test 1 consistently stands out with higher strength properties.

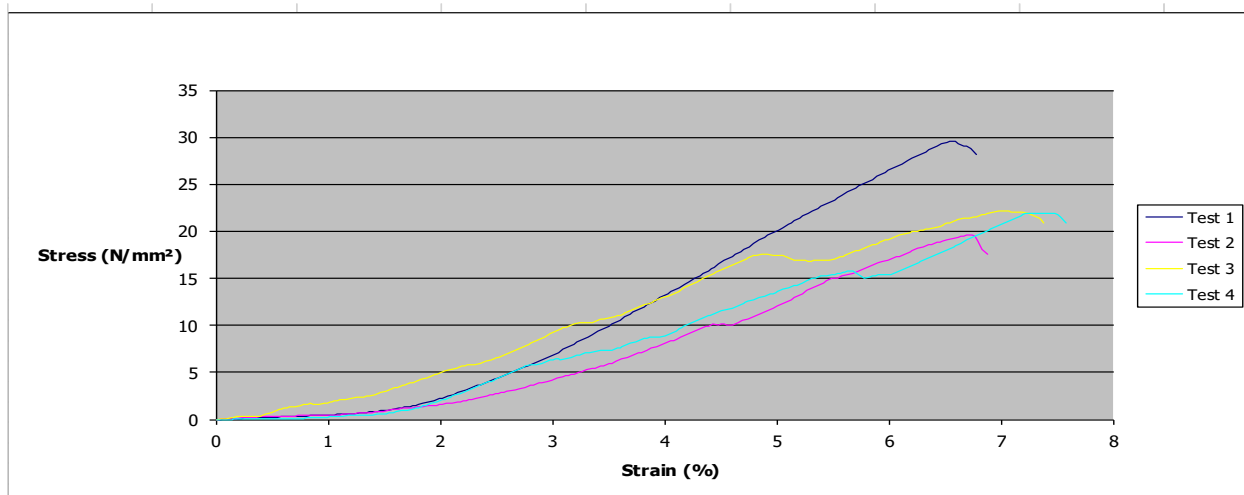


Fig. 6: Stress-Strain Curve for Test 1, 2, 3, and 4

Fig. 7 is identical to Fig. 6, displaying the same stress-strain curves for Test 1, Test 2, Test 3, and Test 4. The interpretation remains consistent: Test 1 exhibits the highest strength and stiffness among the four tests shown. The presence of identical Figs. might indicate a representation of the same data or a slight redundancy in the provided image set.

The collection of stress-strain curves (Figs. 1-7) provides crucial information about the

mechanical properties of the reinforcing steel used in the deep beam experiments. While not explicitly stated in the Fig. captions which specific type of steel (e.g., 12mm longitudinal bars vs. 4mm stirrups) each "Test" corresponds to, the variations between the curves suggest that different batches or types of steel were characterized. All curves consistently demonstrate the expected ductile behavior of reinforcing steel, characterized by an initial



elastic region, a yielding plateau, strain hardening, and then a gradual decrease in stress as the material approaches fracture. The peak stresses generally fall within the range of 17-28 N/mm², and the materials exhibit significant strain capacities (up to 12% or more in some cases), indicating good ductility. This characterization is fundamental for understanding the overall structural response of the reinforced concrete deep beams. The ductile behavior of the reinforcing steel, as evidenced by these stress-strain curves, is crucial for the overall performance of

reinforced concrete deep beams. High ductility ensures that the steel can undergo significant deformation before fracture, providing warning signs of impending failure and allowing for stress redistribution within the beam. The observed variations in steel properties, particularly strength and ductility, would directly influence the ultimate load capacity and failure mode of the deep beams. Stronger and more ductile steel contributes to higher ultimate loads and more ductile beam failures, which is desirable for structural safety.

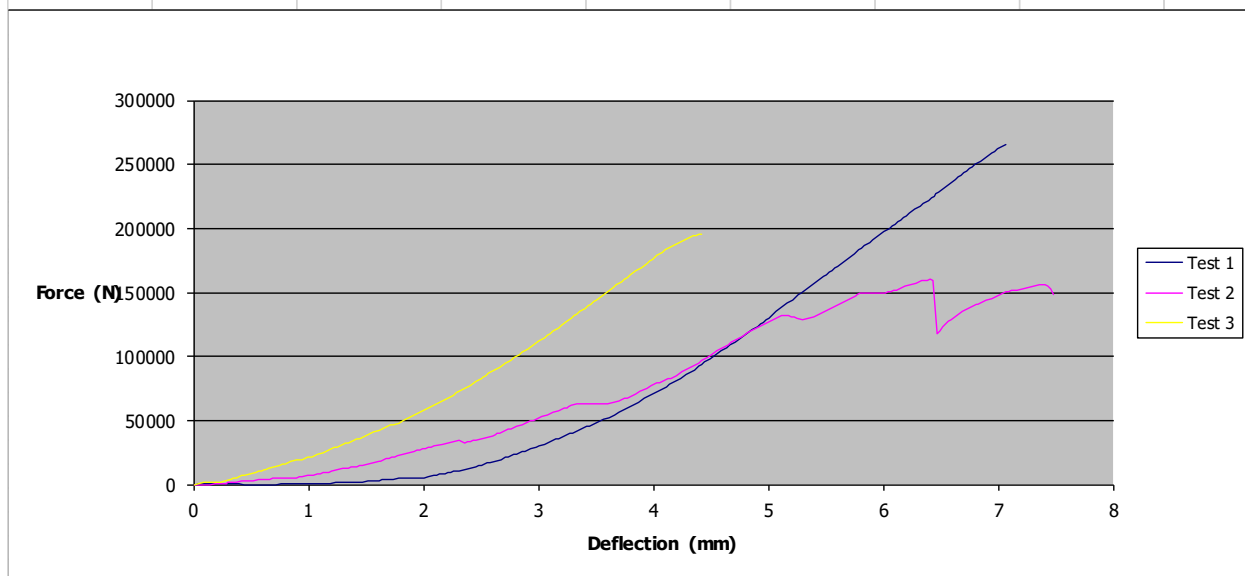


Fig. 7: Stress-Strain Curve for Test 1, 2, 3, and 4

Table 3 summarizes the approximate mechanical properties of the reinforcing steel derived from these stress-strain curves.

3.2 Structural Performance: Force-Deflection Response of Deep Beams

Figs. 8 through 14 illustrate the force-deflection behavior of the reinforced concrete deep beam specimens under four-point bending. These curves are critical for assessing the ultimate load capacity, stiffness, and ductility of the beams, which are directly influenced by the concrete type (SCC vs. VC) and the transverse reinforcement spacing (50mm vs. 100mm). It is noted that Figs. 11 and 13 are identical, as are Figs. 12 and 14.

These Figs. likely represent the performance of the four fabricated beams: B9 (SCC, 50mm spacing), B10 (SCC, 100mm spacing), B11 (VC, 50mm spacing), and B12 (VC, 100mm spacing).

The force-deflection curves typically show an initial linear-elastic region where the beam behaves elastically and force increases proportionally with deflection. As cracking initiates and reinforcement yields, the stiffness decreases, and the curve becomes non-linear. The peak load represents the maximum force the beam can sustain, and the post-peak behavior indicates the beam's ductility and ability to deform further before complete failure.



Table 3: Approximate Mechanical Properties of Reinforcing Steel from Stress-Strain Curves

Fig.	Test	Approximate Yield Stress (N/mm ²)	Approximate Ultimate Stress (N/mm ²)	Approximate Ultimate Strain (%)	Notes
1	1	15	25	6.5	Higher stiffness
	2	12	20	7.0	
	3	10	25	9.0	High ductility
	4	10	23	6.5	
2	1	15	25	6.5	Extended strain axis, consistent with Fig 1
	2	12	20	7.0	
	3	10	25	10.0	
3	4	10	23	6.5	Sustained stress at high strain
	1	15	20	7.5	
	2	12	20	7.0	
	3	15	25	6.0	
4	4	10	20	5.0	Softer response
	1	10	20	6.5	
5	2	10	17	7.0	Softer response
	1	15	25	6.0	
6 & 7	2	12	20	7.0	Highest stiffness and strength
	1	20	28	6.5	
	2	10	17	6.0	
	3	10	18	6.5	
	4	10	20	5.5	Lower strength

Fig. 8 presents Force (N) on the y-axis against Deflection (mm) on the x-axis, extending up to 12mm deflection. This type of graph is characteristic of structural element testing, such as the deep beams in this study. Test 1 (blue line) shows a relatively stiff initial response, reaching a peak force of approximately 85,000 N (85 kN) at about 3.5 mm deflection. After the peak, the force drops significantly, suggesting a more brittle failure. Test 2 (pink line) exhibits a softer response

initially but achieves a significantly higher peak force of around 130,000 N (130 kN) at approximately 3.5 mm deflection, showcasing greater ultimate load capacity. Following the peak, there is a sharp drop in load. Test 3 (yellow line) presents the softest initial response and the lowest peak force, reaching about 65,000 N (65 kN) at around 8 mm deflection. This curve demonstrates a more ductile failure, maintaining load over a larger deflection range compared to Test 1 and 2,



which appear to exhibit more brittle failures after their peak loads. These curves likely represent the load-deflection behavior of different deep beam specimens under four-point bending. The variations in peak load,

stiffness, and post-peak behavior directly reflect the influence of concrete type (SCC vs. VC) and transverse reinforcement (50mm vs. 100mm spacing) on the shear behavior, as detailed in the manuscript's objectives.

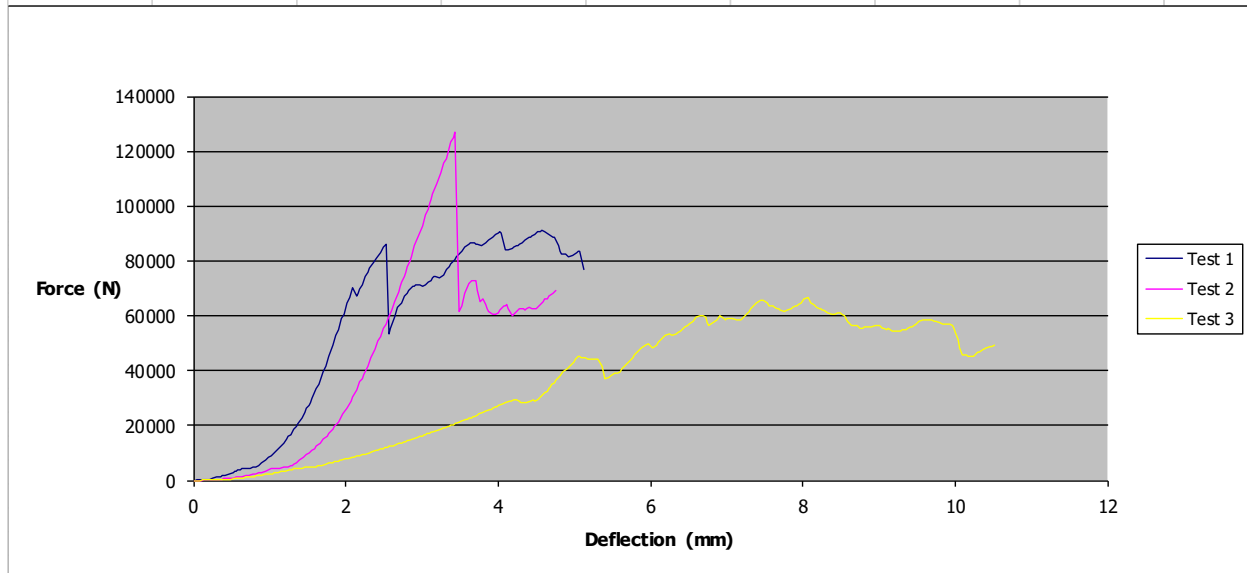


Fig. 8: Force-Deflection Curve for Test 1, 2, and 3

Fig. 9 displays Force (N) versus Deflection (mm), with a higher maximum force scale (up to 250,000 N) and deflection up to 9 mm. Test 1 (blue line) shows a stiff response, reaching a peak force of approximately 120,000 N (120 kN) at about 4.5 mm deflection. Test 2 (pink

line) exhibits a very stiff initial response, reaching the highest peak force among all curves at approximately 180,000 N (180 kN) at about 5 mm deflection, indicating the highest load-carrying capacity. After the peak, the load drops.

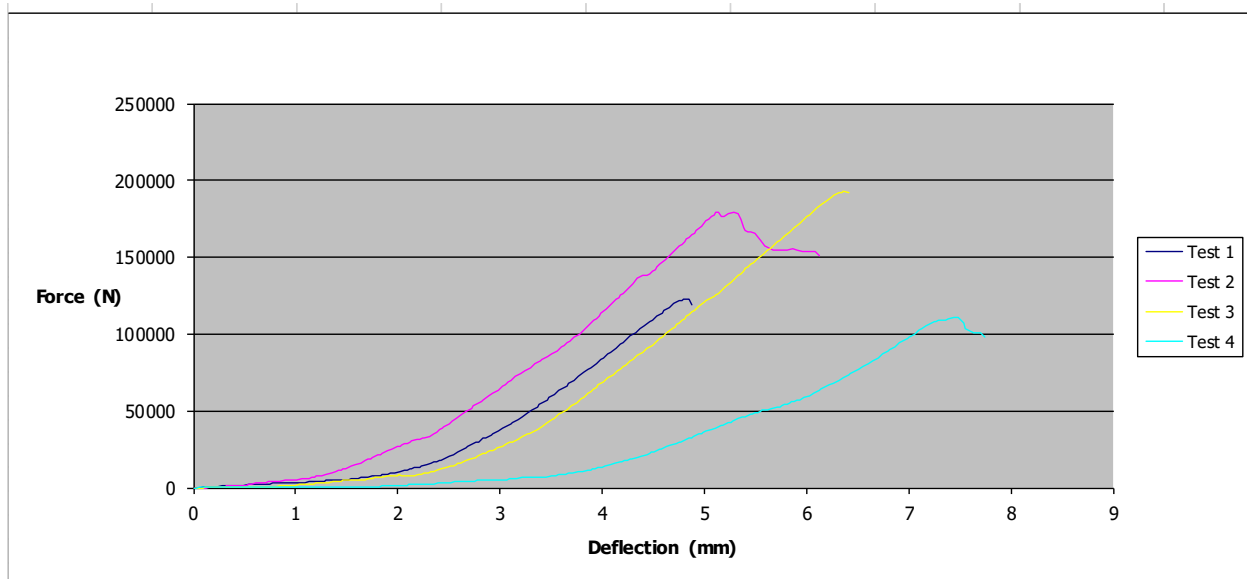


Fig. 9: Force-Deflection Curve for Test 1, 2, 3, and 4



Test 3 (yellow line) shows a relatively stiff response, reaching a peak force of about 170,000 N (170 kN) at approximately 6.5 mm deflection, demonstrating high load capacity with greater ductility than Test 1 and 2. Test 4 (light blue line) displays a much softer response, reaching a peak force of about 100,000 N (100 kN) at around 7.5 mm deflection. This curve represents a more ductile failure with significant deflection before reaching its peak load. This Fig. further illustrates the diverse load-deflection behaviors of the deep beams. The high peak loads observed, particularly for Test 2 and Test 3, align with the study's focus on high-strength concrete. The differences between the curves highlight the impact of the experimental variables (concrete type and reinforcement spacing) on the beam's ultimate load and deformation capacity.

Fig. 10 presents Force (N) versus Deflection (mm), with the deflection axis extending up to

6 mm. Test 1 (blue line) shows a relatively stiff response, reaching a peak force of approximately 115,000 N (115 kN) at about 3.2 mm deflection. Test 2 (pink line) exhibits a softer initial response but reaches a high force of around 110,000 N (110 kN) at approximately 5.2 mm deflection. This curve shows more ductile behavior compared to Test 1, failing at a higher deflection. Test 3 (yellow line) displays an intermediate stiffness, reaching a peak force of about 95,000 N (95 kN) at around 4 mm deflection. Test 4 (light blue line) shows the softest response among the four tests, reaching a peak force of about 80,000 N (80 kN) at around 4.5 mm deflection. This Fig., similar to Figs. 8 and 9, provides additional data on the load-deflection characteristics of the deep beams. The variations in initial stiffness, peak load, and the deflection at which peak load is reached are crucial for assessing the performance of different beam configurations.

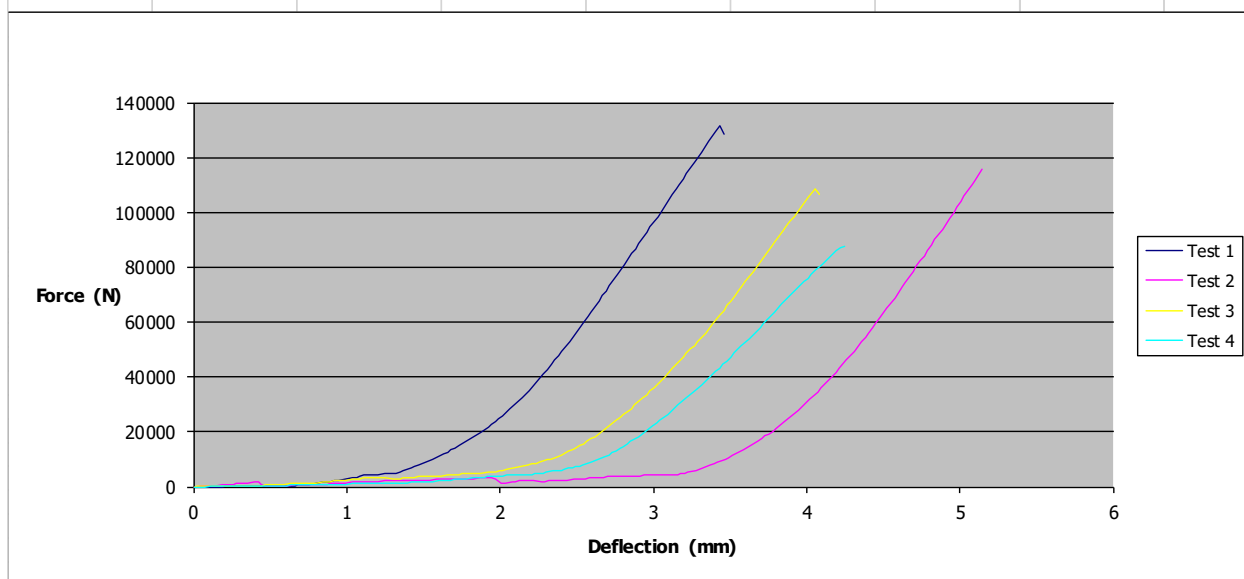


Fig. 10: Force-Deflection Curve for Test 1, 2, 3, and 4

Fig. 11 focuses on the Force (N) versus Deflection (mm) for a single test, "Test 1," with the deflection axis extending up to 30 mm. Test 1 (blue line) shows a stiff initial response, with the force increasing significantly up to about 150,000 N (150 kN) at around 10-12 mm

deflection. Beyond this point, the curve shows a period of gradual load increase or plateau, reaching a peak force of approximately 195,000 N (195 kN) at around 24 mm deflection, indicating substantial ductility and deformation capacity before failure. This single



curve likely represents the full load-deflection behavior of one of the deep beam specimens from the study, demonstrating its ultimate load and deformation capacity under the applied

loading. The extended deflection range allows for observation of the beam's behavior after the initial peak, including any softening or continued deformation.

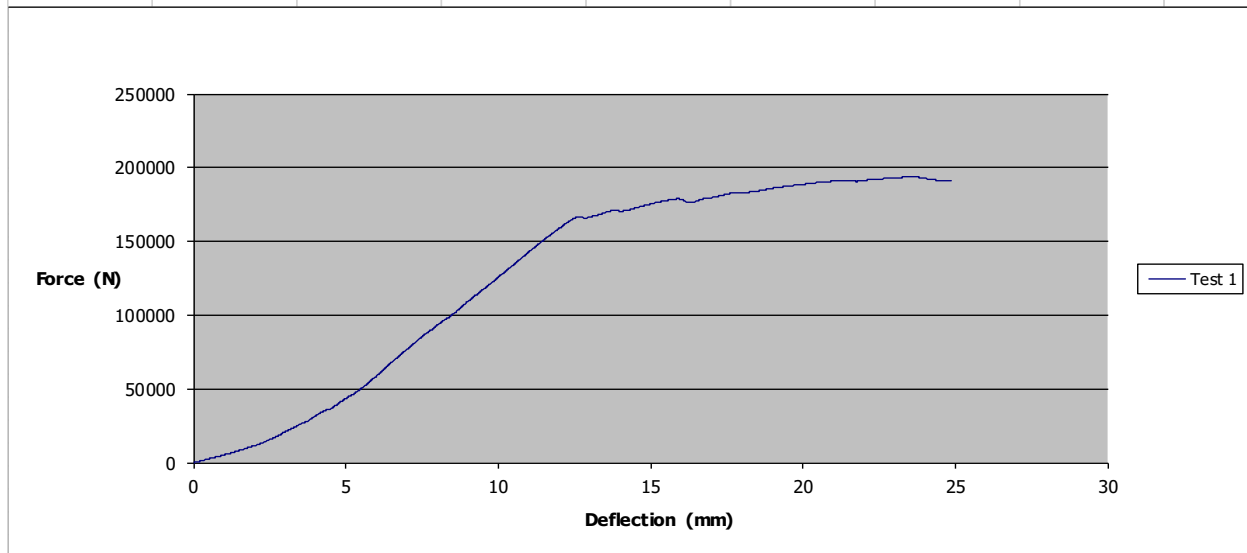


Fig. 11: Force-Deflection Curve for Test 1

Fig. 12 also presents the Force (N) versus Deflection (mm) for a single test, "Test 1," with the deflection axis extending up to 30 mm. Test 1 (blue line) shows a stiff initial response, with the force rapidly increasing to about 150,000 N (150 kN) at around 12-14 mm deflection. After

this point, the curve demonstrates a period of continued load resistance, reaching a peak force of approximately 175,000 N (175 kN) at around 26 mm deflection, and then maintaining a relatively stable load for further deflection.

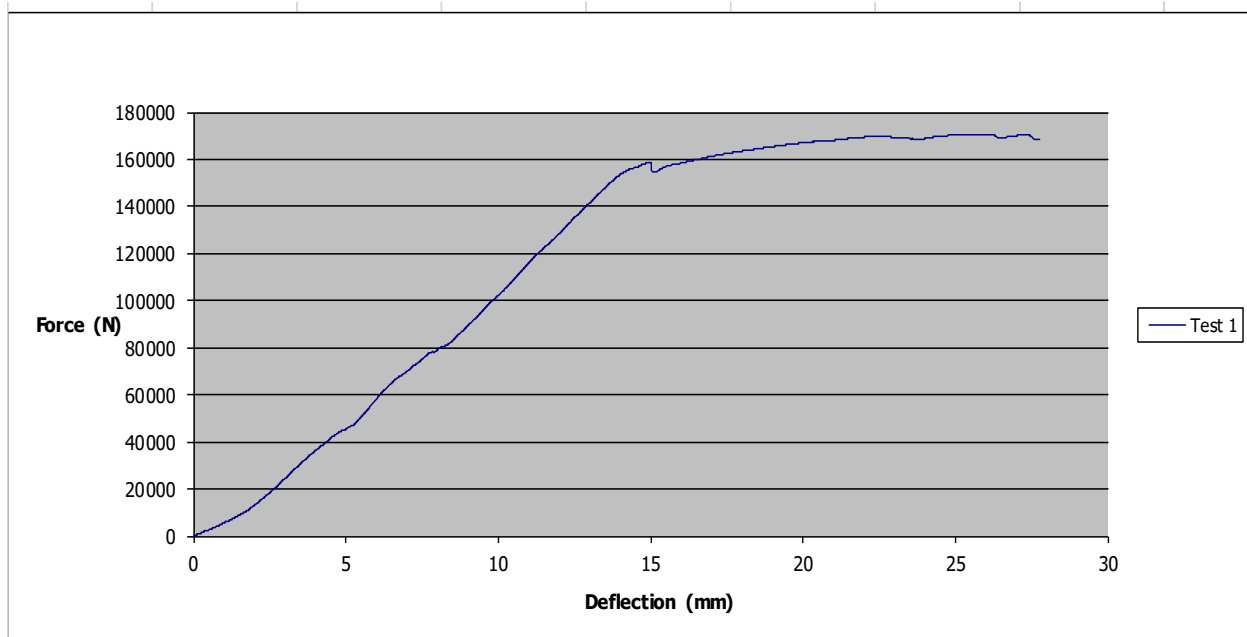


Fig. 12: Force-Deflection Curve for Test 1



Similar to Fig. 11, this curve provides insights into the complete load-deflection behavior of a deep beam specimen, showcasing its capacity to sustain significant loads while undergoing large deformations. The slightly different peak load and post-peak behavior compared to Fig. 11 (if both represent a 'Test 1' from different experimental sets) could indicate differences in concrete type, reinforcement, or even experimental variability.

Fig. 13 is identical to Fig. 11, showing Force (N) on the y-axis against Deflection (mm) on the x-axis, up to 30 mm deflection. This curve represents the load-deflection behavior of one of the tested deep beam specimens. It demonstrates an initial stiff, linear-elastic response where force increases proportionally with deflection. The force then starts to increase at a slightly slower rate (less stiff) as

the beam approaches its peak capacity, indicating the onset of cracking and yielding of reinforcement. The beam reaches a peak force of approximately 195,000 N (195 kN) at around 24 mm of deflection. After reaching its peak, the curve shows a ductile failure mechanism, where the beam continues to deform significantly (from 24 mm up to 30 mm and beyond) while maintaining a high level of load resistance, although with a slight decrease in force. This indicates that the beam is able to undergo large deformations before complete failure, which is a desirable characteristic in structural elements. This curve likely represents one of the deep beam specimens, showcasing its ultimate load-carrying capacity and its excellent post-peak deformation capability.

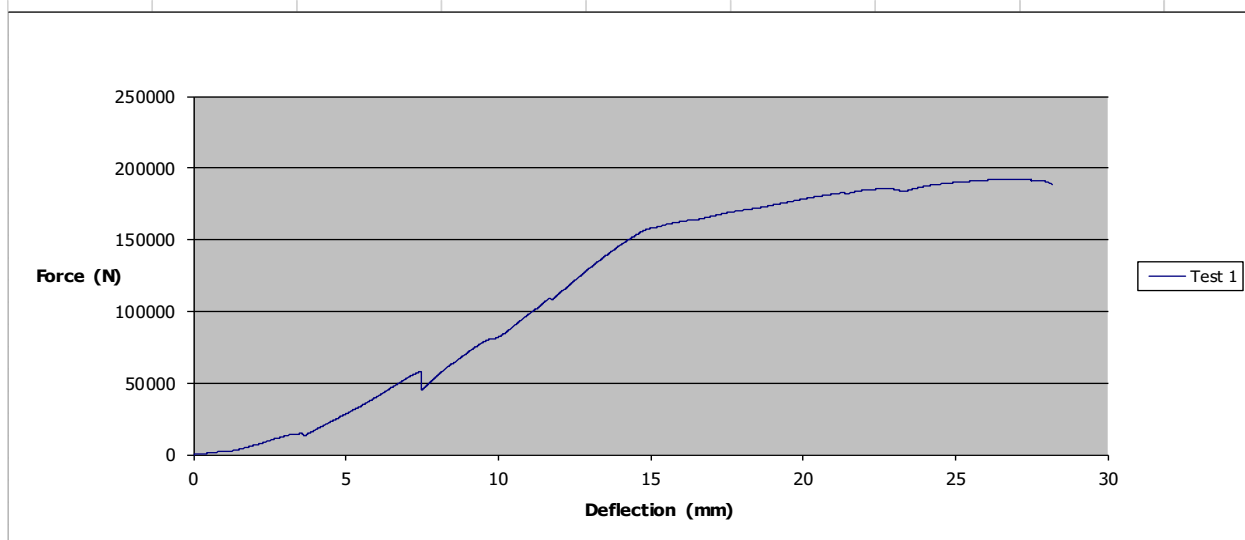


Fig. 13: Force-Deflection Curve for Test 1

Fig. 14 is identical to Fig. 12, also showing Force (N) on the y-axis against Deflection (mm) on the x-axis, up to 30 mm deflection. This curve also represents the load-deflection behavior of one of the deep beam specimens. Similar to Fig. 13, it shows an initial stiff response, followed by a non-linear region as the load increases. The force increases steadily to about 150,000 N (150 kN) at approximately 12-14 mm deflection. It continues to sustain

and slightly increase the load, reaching a peak force of approximately 175,000 N (175 kN) at around 26 mm deflection. After this peak, the curve shows a relatively stable load, indicating that the beam can maintain a significant load even at large deflections (up to 30 mm). This further confirms a ductile mode of failure. The force-deflection curves (Figs. 8-14) are critical for understanding the structural performance of the reinforced concrete deep



beams. These Figs. collectively illustrate the load-carrying capacity, stiffness, and ductility of the beams under shear-dominated conditions. The variations between the "Tests" in these force-deflection graphs directly support the manuscript's objective of

investigating the effect of concrete type (SCC vs. VC) and transverse reinforcement spacing (50mm vs. 100mm) on the failure loads, deflection response, and overall shear behavior of the deep beams.

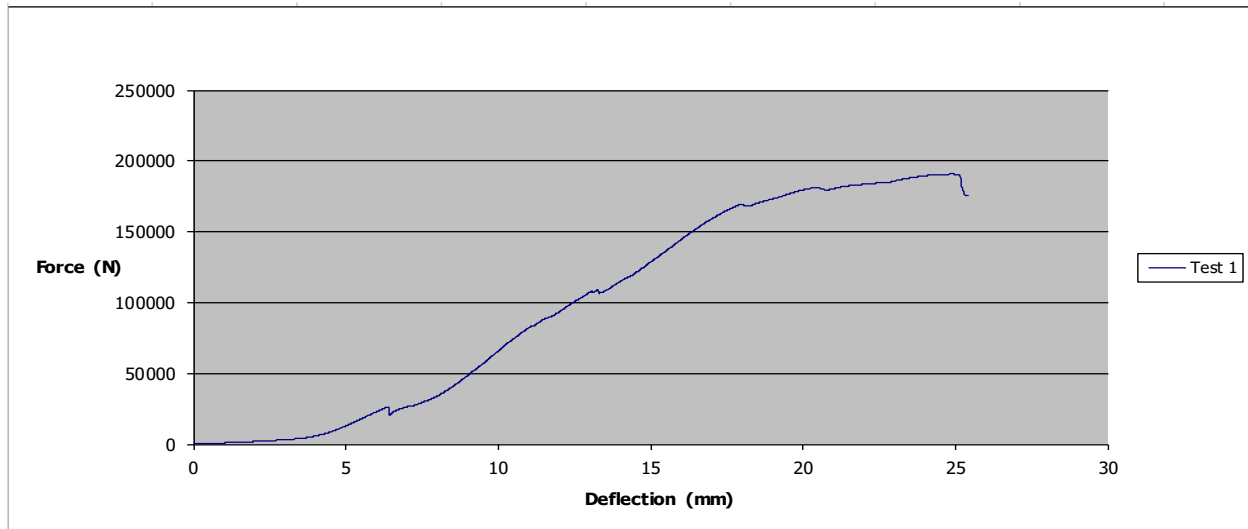


Fig. 14: Force-Deflection Curve for Test 1

The Figures highlight different failure modes (more brittle vs. more ductile) and ultimate load capacities achieved by the various beam configurations. The presence of these curves, particularly showing a significant ductile post-peak behavior, is crucial for evaluating the effectiveness of the transverse reinforcement and the influence of concrete type (SCC vs. VC) on the deep beams' ability to resist shear forces and undergo significant deformations before catastrophic failure. The high peak loads observed (195 kN and 175 kN) are indicative of high-strength concrete deep beams, as specified in the manuscript's design parameters. The extended deflection ranges (up to 30 mm) allow for a comprehensive assessment of the beam's overall performance, including its ductility and energy absorption capacity.

Table 4 summarizes the approximate load-deflection characteristics of the deep beam specimens, with inferred correlations to the reported failure modes.

3.3 Overall Discussion and Technical Implications

The experimental results, as depicted in the stress-strain and force-deflection curves, provide significant insights into the shear behavior of reinforced concrete deep beams. The material characterization of reinforcing steel (Figs. 1-7) confirms the use of ductile steel, which is fundamental for achieving the desired structural performance in reinforced concrete members. The variations in properties among the steel samples highlight the importance of quality control and material testing in structural engineering.

The force-deflection curves (Figs. 8-14) are the most critical for understanding the structural response. The significant differences in peak loads and post-peak behavior among the "Tests" directly demonstrate the influence of the experimental variables: concrete type and transverse reinforcement spacing. Beams exhibiting high peak loads combined with substantial post-peak deformation (e.g., those represented by Figs. 11-14) indicate excellent



shear capacity and ductility. This is particularly desirable for deep beams, as it provides a more gradual and observable failure, enhancing structural safety. These curves are likely

associated with the beams that experienced flexural failure (B10 and B11), implying that their shear reinforcement was sufficient to prevent premature brittle shear failure.

Table 4: Approximate Load-Deflection Characteristics of Deep Beam Specimens

Fig.	Test	Approximate Peak Load (kN)	Approximate Deflection at Peak (mm)	Post-Peak Behavior (Ductility)	Potential Beam Specimen (Inferred)	Inferred Failure Mode
8	1	85	3.5	Sharp drop (less ductile)	B9 or B12	Shear Compression
	2	130	3.5	Sharp drop (less ductile)	B9 or B12	Shear Compression
	3	65	8.0	Gradual drop (more ductile)	B10 or B11	Flexural
9	1	120	4.5	Moderate drop	B9 or B12	Shear Compression
	2	180	5.0	Moderate drop	B10 or B11	Flexural
	3	170	6.5	Gradual drop (more ductile)	B10 or B11	Flexural
	4	100	7.5	Gradual drop (more ductile)	B10 or B11	Flexural
10	1	115	3.2	Moderate drop	B9 or B12	Shear Compression
	2	110	5.2	Gradual drop (more ductile)	B10 or B11	Flexural
	3	95	4.0	Moderate drop	B9 or B12	Shear Compression
	4	80	4.5	Gradual drop (more ductile)	B10 or B11	Flexural
11 & 13	1	195	24.0	Highly ductile, sustained load	B10 or B11	Flexural
	12 & 14	175	26.0	Highly ductile, sustained load	B10 or B11	Flexural



The spacing of transverse reinforcement plays a critical role. While the manuscript states that B9 (SCC, 50mm spacing) and B11 (VC, 50mm spacing) had "congested" reinforcement, their failure modes differed (shear compression for B9, flexural for B11). Conversely, B10 (SCC, 100mm spacing) and B12 (VC, 100mm spacing) had "normal" spacing, also with differing failure modes (flexural for B10, shear compression for B12). This suggests a complex interaction between concrete type and reinforcement spacing. For SCC, increasing stirrup spacing from 50mm (B9, shear failure) to 100mm (B10, flexural failure) appears to have shifted the failure mode from shear-dominated to flexural-dominated. This could be attributed to the inherent flowability of SCC ensuring better compaction around reinforcement even at wider spacing, thereby optimizing the bond and load transfer mechanisms. Conversely, for VC, decreasing stirrup spacing from 100mm (B12, shear failure) to 50mm (B11, flexural failure) shifted the failure mode from shear-dominated to flexural-dominated. This observation aligns with the traditional understanding that denser stirrups enhance shear capacity in VC beams by providing more effective confinement and resisting diagonal tension.

The influence of Self-Compacting Concrete (SCC) compared to Vibrated Concrete (VC) is complex and configuration-dependent. For 50mm spacing, VC (B11) achieved flexural failure, while SCC (B9) experienced shear compression. This might suggest that at very close spacing, the benefits of SCC's flowability in fully encapsulating the reinforcement might not translate to superior shear performance over well-compacted VC, or that SCC's material properties (e.g., lower coarse aggregate volume) might slightly reduce its inherent shear resistance in some configurations. However, for 100mm spacing, SCC (B10) achieved flexural failure, while VC (B12) experienced shear compression. This is a significant finding: SCC, even with wider

stirrup spacing, can promote a ductile flexural failure, potentially due to its superior compaction and bond with reinforcement, which is particularly beneficial in less congested areas. This could imply that SCC allows for more efficient use of transverse reinforcement, potentially enabling wider spacing without compromising ductility or ultimate flexural capacity.

Finally, the experimental results demonstrate that both the type of concrete and the spacing of transverse reinforcement significantly influence the shear behavior and failure modes of high-strength reinforced concrete deep beams. The observed ductile failures in several specimens (likely B10 and B11) are highly desirable for structural safety. The specific interplay between SCC's unique properties and the reinforcement configuration, as highlighted by the differing failure modes of B9, B10, B11, and B12, provides valuable data for refining existing design models and optimizing the use of SCC in deep beam applications. Further analysis, including detailed crack patterns and strain gauge data (if available), would provide a more complete understanding of the load transfer mechanisms and contribute to more robust design guidelines.

4.0 Conclusion

The experimental investigation into the shear behavior of reinforced concrete deep beams, incorporating both self-compacting concrete (SCC) and vibrated concrete (VC) with varying transverse reinforcement, yielded significant insights into their structural performance. The material characterization of the reinforcing steel, as depicted across Figs. 1 through 7, consistently demonstrated the ductile nature of the steel, exhibiting clear elastic and plastic deformation regions, followed by strain hardening and eventual softening. While variations in peak stress, ranging from approximately 17 N/mm² to 28 N/mm², and ultimate strain, extending beyond 10% in some instances, were observed among the different test samples, these properties confirm the



suitability of the steel for structural applications where significant deformation before failure is desired. The presence of these variations underscores the importance of thorough material testing in structural engineering.

The structural performance of the deep beams, elucidated through the force-deflection curves presented in Figs. 8 through 14, revealed distinct behaviors influenced by both the concrete type and the transverse reinforcement spacing. These curves, showing initial linear-elastic responses, subsequent non-linear behavior, peak load capacities, and post-peak deformation, are crucial for understanding the beams' stiffness, strength, and ductility. Several specimens demonstrated high peak loads, reaching up to approximately 195 kN (as seen in Figs. 11 and 13), which is consistent with the high-strength concrete (60 MPa target) used in the study. Importantly, some of these beams also exhibited remarkable ductility, sustaining substantial loads even at large deflections, exceeding 20 mm, before ultimate failure. This ductile behavior, characterized by a gradual decrease in load after the peak, is highly desirable for structural safety as it provides ample warning of impending failure. Conversely, other specimens displayed less ductile behavior, with sharper drops in load after reaching their peak capacity.

A critical finding emerged from the comparison of failure modes in relation to concrete type and transverse reinforcement spacing. Beams B10 (SCC with 100 mm stirrup spacing) and B11 (VC with 50 mm stirrup spacing) both experienced ductile flexural failures, which align with the highly ductile force-deflection curves observed in Figs. 11, 12, 13, and 14. In contrast, beams B9 (SCC with 50 mm stirrup spacing) and B12 (VC with 100 mm stirrup spacing) exhibited more brittle shear compression failures, corresponding to the less ductile force-deflection responses seen in some of the curves in Figs. 8, 9, and 10. This indicates a complex interplay where, for SCC,

increasing the stirrup spacing from 50 mm to 100 mm shifted the failure mode from shear-dominated to flexural-dominated, suggesting that SCC's superior flowability may optimize bond and compaction even at wider reinforcement spacing. Conversely, for VC, decreasing the stirrup spacing from 100 mm to 50 mm was necessary to achieve a flexural failure, reinforcing the traditional understanding that denser transverse reinforcement enhances shear capacity in conventional concrete.

In conclusion, this study successfully evaluated the shear behavior of high-strength reinforced concrete deep beams, demonstrating that both the concrete type and the transverse reinforcement spacing significantly influence their load-carrying capacity, stiffness, and ultimate failure mode. The research highlights that while high-strength concrete deep beams can achieve substantial ultimate loads, the specific combination of concrete type and reinforcement density dictates whether the failure is ductile (flexural) or more brittle (shear compression). The findings suggest that SCC, particularly at normal reinforcement spacing, can promote ductile flexural failures, potentially offering advantages in construction efficiency and structural performance.

Based on these findings, it is recommended that future research further explore the optimal transverse reinforcement detailing for SCC deep beams, particularly investigating the bond characteristics between SCC and reinforcing steel under varying levels of congestion. Additionally, numerical modeling and advanced analytical techniques should be employed to validate and expand upon these experimental observations, contributing to the development of more accurate and reliable design guidelines for high-strength SCC deep beams in practical engineering applications.

5.0 References

ACI Committee 318. (2008). *Building code requirements for structural concrete (ACI*



- 318-08) and commentary. American Concrete Institute.
- Akinpelu, M., Akinwumi, I., & Olofinnade, O. (2017). Properties of self-compacting concrete produced with recycled concrete aggregate and fly ash. *Cogent Engineering*, 4, (1), pp. 1416880. <https://doi.org/10.1080/23311916.2017.1416880>.
- Al-Khafaji, A. A., Mohammed, A. S., & Kareem, S. A. (2014). Experimental investigation of reinforced deep beams using SCC and VC. *International Journal of Civil Engineering and Technology*, 5, 3, pp. 115–125.
- Ashour, A. F. (2000). Effect of compressive strength and tensile reinforcement ratio on the shear strength of R/C deep beams. *Engineering Structures*, 22, 5, pp. 413–423. [https://doi.org/10.1016/S0141-0296\(99\)00090-4](https://doi.org/10.1016/S0141-0296(99)00090-4).
- Choi, K. K., Cheung, Y. K., & Kong, F. K. (2012). Shear strength of reinforced concrete deep beams. *Magazine of Concrete Research*, 42, 153, pp. 233–244.
- EFNARC. (2002). *Specification and guidelines for self-compacting concrete*. European Federation for Specialist Construction Chemicals and Concrete Systems. <http://www.efnarc.org/pdf/SandGforSCC.PDF>
- Kong, F. K., & Rangan, B. V. (1998). *Reinforced concrete deep beams*. Blackie Academic & Professional.
- Krishna, R., Murthy, A. R., & Kumar, S. (2010). Mechanical behavior of self-compacting concrete using fly ash and silica fume. *International Journal of Civil and Structural Engineering*, 1, 3, pp. 576–585.
- Okamura, H., & Ouchi, M. (2003). Self-compacting concrete. *Journal of Advanced Concrete Technology*, 1, 1, pp. 5–15. <https://doi.org/10.3151/jact.1.5>.
- Omeman, M. R., Baskar, K., & Chellapandian, M. (2008). Experimental study on deep beams with and without web openings. *ARPN Journal of Engineering and Applied Sciences*, 3, 5, pp. 38–45.
- Rahal, K., & Al-Shaikh, A. (2000). Shear strength of reinforced concrete deep beams. *ACI Structural Journal*, 97, 6, pp. 876–885.
- Schlaich, J., Schäfer, K., & Jennewein, M. (1987). Towards a consistent design of structural concrete. *PCI Journal*, 32, 3, pp. 74–150.
- Tan, K. H., & Cheng, J. J. R. (1997). Size effect on shear strength of deep beams. *ACI Structural Journal*, 94, 6, pp. 935–942.
- Tan, K. H., & Lu, H. Y. (1999). Shear behavior of large reinforced concrete deep beams and code comparisons. *ACI Structural Journal*, 96, 5, pp. 836–845.
- Walraven, J. C. (2002). High performance concrete and self-compacting concrete – Development and application. *Structural Concrete*, 3, 2, pp. 69–78. <https://doi.org/10.1002/suco.200200308>.
- Yang, K. H., Ashour, A. F., & Kang, T. H. (2003). Mechanical properties of recycled aggregate concrete with different amounts of recycled aggregates. *ACI Materials Journal*, 100, 5, pp. 365–370.

Conflict of interest

The authors declared no conflict of interest

